Immunity
Article

Maturation of Lymph Node Fibroblastic Reticular Cells from Myofibroblastic Precursors Is Critical for Antiviral Immunity

Qian Chai,[1,8] Lucas Onder,[1,8] Elke Scandella,[1] Cristina Gil-Cruz,[1] Christian Perez-Shibayama,[1] Jovana Cupovic,[1] Renzo Danuser,[2] Tim Sparwasser,[3] Sanjiv A. Luther,[4] Volker Thiel,[1,5] Thomas Rülicke,[6] Jens V. Stein,[2] Thomas Hehlgans,[7] and Burkhard Ludewig[1,*]

[1]Institute of Immunobiology, Kantonal Hospital St. Gallen, 9007 St. Gallen, Switzerland
[2]Theodor Kocher Institute, 3012 Bern, Switzerland
[3]Institute of Infection Immunology, TWINCORE, Hannover Medical School, 30625 Hannover, Germany
[4]École Polytechnique Fédérale de Lausanne, 1015 Lausanne, Switzerland
[5]VetSuisse Faculty, University of Zurich, 8006 Zurich, Switzerland
[6]Institute of Laboratory Animal Science and Biomodels Austria, University of Veterinary Medicine Vienna, 1210 Vienna, Austria
[7]University of Regensburg, 93042 Regensburg, Germany
[8]These authors contributed equally to this work
*Correspondence: burkhard.ludewig@kssg.ch
http://dx.doi.org/10.1016/j.immuni.2013.03.012

SUMMARY

The stromal scaffold of the lymph node (LN) paracortex is built by fibroblastic reticular cells (FRCs). Conditional ablation of lymphotoxin-β receptor (LTβR) expression in LN FRCs and their mesenchymal progenitors in developing LNs revealed that LTβR-signaling in these cells was not essential for the formation of LNs. Although T cell zone reticular cells had lost podoplanin expression, they still formed a functional conduit system and showed enhanced expression of myofibroblastic markers. However, essential immune functions of FRCs, including homeostatic chemokine and interleukin-7 expression, were impaired. These changes in T cell zone reticular cell function were associated with increased susceptibility to viral infection. Thus, myofibroblasic FRC precursors are able to generate the basic T cell zone infrastructure, whereas LTβR-dependent maturation of FRCs guarantees full immunocompetence and hence optimal LN function during infection.

INTRODUCTION

Lymph nodes (LNs) and other secondary lymphoid organs (SLOs) provide particular microenvironments for optimal induction and control of immune responses (Junt et al., 2008; Mueller and Germain, 2009). These specialized niches are generated and maintained by different sets of vascular and mesenchymal stromal cells (Randall et al., 2008; Turley et al., 2010). The mesenchymal stromal cell network of the LN T cell zone is formed by fibroblastic reticular cells (FRCs) which are characterized by the expression of podoplanin (PDPN), and extracellular matrix proteins such as ERTR-7 and collagen-I (Malhotra et al., 2012). Furthermore, FRCs regulate immune homeostasis and reactivity through the production of homeostatic chemokines, the immune-regulatory cytokine interleukin-7 (IL-7) (Link et al., 2007), and small molecules such as nitric oxide (Lukacs-Kornek et al., 2011; Siegert et al., 2011). However, although LN FRCs are phenotypically well-characterized (Katakai et al., 2004; Malhotra et al., 2012), their development from mesenchymal precursors has remained elusive.

The differentiation of FRCs from their progenitor(s) is thought to be closely linked to lymphoid organogenesis. The early steps of both LN and Peyer's patch (PP) organogenesis involve the appearance of hematopoietic lymphoid tissue inducer (LTi) cells in the respective anlagen (Mebius et al., 1997; Yoshida et al., 1999). Lymphotoxin-β receptor (LTβR) and receptor activator of NF-κB ligand (RANKL)-mediated interaction of LTi cells with mesenchymal stromal cells in the LN or PP anlage is thought to be critical for their further development (van de Pavert and Mebius, 2010; Randall et al., 2008). Indeed, mice lacking LTi cells fail to generate both LNs and PPs (Eberl et al., 2004; Boos et al., 2007) and molecules of the tumor necrosis factor (TNF) family expressed by LTi cells provide essential signals for the developing SLOs (De Togni et al., 1994; Koni et al., 1997; Kong et al., 1999). LTβR engagement on stromal cells appears to be particularly important because the expression of IL-7, C-C motif chemokine 19 (CCL19), and CCL21 generates a positive feedback loop that attracts and activates further LTi cells (Honda et al., 2001; Ohl et al., 2003). Mesenchymal stromal cells interacting with LTi cells during prenatal stages of SLO development are commonly referred to as lymphoid tissue organizer (LTo) cells and have been described as intercellular adhesion molecule 1 (ICAM-1)- and vascular cell adhesion molecule 1 (VCAM-1)-expressing cells that appear around embryonic day (E) 16 in the murine LN anlage (Cupedo et al., 2004c; White et al., 2007). Gene-expression analysis revealed that these cells provide molecules involved in LN organogenesis including LTβR, RANKL, CCL19, CCL21, CXCL13, and IL-7 (Cupedo et al., 2004c; Bénézech et al., 2010). However, neither global gene ablation of LTβR-ligands (De Togni et al., 1994; Koni et al., 1997) or the LTβR itself (Fütterer et al., 1998), nor LTβR expression on mesenchymal

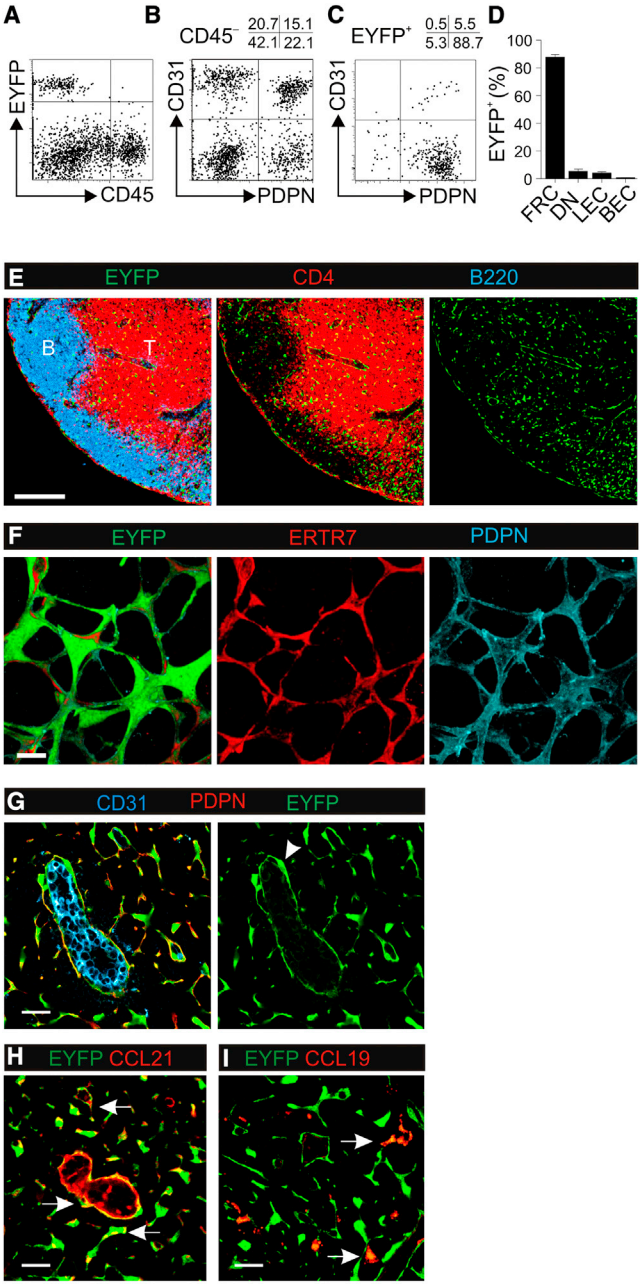

Figure 1. *Ccl19-cre* Transgene Expression in LN Stromal Cells

(A) LN cell suspensions from 6-week-old *Ccl19-cre* × *R26-eyfp* mice were depleted of $CD45^+$ cells, and EYFP expression was determined by flow cytometry.

(B) Representative dot plot analysis with quadstat values of CD31 and PDPN expression in $CD45^-$ inguinal LN stromal cells.

(C) Dot plot analysis including quadstat values of CD31 and PDPN expression in $CD45^-EYFP^+$ LN stromal cells.

(D) EYFP expression in $CD45^-$ LN stromal cell populations ($PDPN^+CD31^-$ fibroblastic reticular cells [FRC]; $PDPN^-CD31^-$ double-negative [DN] cells; $PDPN^+CD31^+$ lymphatic endothelial cells [LECs]; $PDPN^-CD31^+$ blood endothelial cells [BEC]). Inguinal LNs from individual mice were pooled, mean values ± SEM from 15 mice analyzed in three independent experiments.

(E) Confocal microscopic analysis of an *Ccl19-cre* × *R26-eyfp* inguinal LN section by using antibodies against the indicated markers, merged channels in left panel; scale bar represents 200 μm.

(F) 3D reconstruction of T cell zone FRC network, merged channels in left panel, scale bar = 10 μm.

(G) EYFP expression in perivascular FRCs (arrow); scale bar represents 20 μm.

(H and I) Expression of the homeostatic chemokines CCL21 (H, arrows) and CCL19 (I, arrows) in $EYFP^+$ FRCs in T cell zones of *Ccl19-cre* × *R26-eyfp* inguinal LNs; scale bar represents 20 μm. See also Figure S1.

stromal cells of the LN anlage (Cupedo et al., 2004c; White et al., 2007; Bénézech et al., 2010) has allowed for the determination of the developmental window of LTβR-dependent mesenchymal LTo cell stimulation that is critical for LN or PP development.

Deletion of genes in a cell-specific and spatiotemporally controlled manner can be achieved by utilizing the Cre-*loxP* system. Here, we report the generation of a bacterial artificial chromosome (BAC)-transgenic mouse model that utilizes the *Ccl19* promoter to target the Cre recombinase specifically to mesenchymal stromal cells of the developing LN and to FRCs and FRC-like cells in adult LNs and PPs, respectively. Surprisingly, ablation of the LTβR on *Ccl19-cre*$^+$ mesenchymal stromal cells did not abrogate LN development. Moreover, although the maturation of LN FRCs from myofibroblastic precursors was blocked in *Ccl19-cre* × *Ltbr*$^{fl/fl}$ mice, the basic infrastructure of the adult LN with T and B cell zone segregation and a functional conduit system was established. However, *Ccl19-cre* × *Ltbr*$^{fl/fl}$ mice were immunodeficient because myofibroblastic FRC precursors were devoid of essential immune-stimulatory properties such as production of homeostatic chemokines and IL-7. Moreover, conditionally FRC-deficient animals showed an impaired resistance to viral infection, indicating that LTβR-mediated FRC maturation is critical for the maintenance of immunocompetence.

RESULTS

Genetic Targeting of LN FRCs

Currently, LN FRCs are defined as $PDPN^+CD31^-$ stromal cells in the T cell zone and interfollicular regions expressing smooth muscle actin (SMA) and the extracellular matrix protein ERTR7 (Link et al., 2007; Malhotra et al., 2012). However, neither of these markers is truly FRC-specific. For example, PDPN is expressed on different stromal cell populations (Malhotra et al., 2012) and hence *Pdpn-cre* transgenes target both $PDPN^+CD31^-$ FRCs and $PDPN^+CD31^+$ lymphatic endothelial cells (LECs) (Onder et al., 2011). Here, we utilized the *Ccl19* promoter to direct Cre recombinase expression to LN FRCs. To silence the *Ccl21* gene, which is in close proximity to the *Ccl19* locus, the murine *Ccl21* gene was replaced by the human *CD8* gene in the BAC construct. Crossing of transgenic lines with *R26-eyfp* reporter mice (Srinivas et al., 2001) facilitated screening for founders with exclusive transgene expression in nonhematopoietic cells (Figure 1A; see also Figures S1A and S1B available online). Because two out of seven founder lines showed identical stromal cell-specific transgene expression, all further analyses were performed with founder line 1 designated as *Ccl19-cre*. Staining of $CD45^-$ LN cells with antibodies against PDPN and CD31 revealed a normal LN stromal cell composition in *Ccl19-cre* × *R26-eyfp* mice (Figure 1B). Importantly, FRC specificity was high with 80%–90% of the EYFP signal being directed to the $PDPN^+CD31^-$ fraction (Figures 1C and 1D). In situ analysis using

confocal laser scanning microscopy revealed that *Ccl19-cre*$^+$ cells were found mainly in the T cell zone and in interfollicular regions of the LN (Figure 1E). Three-dimensional (3D) reconstruction of high-resolution microscopic analyses showed that the transgene was expressed uniformly in the PDPN$^+$ERTR7$^+$ reticular T cell zone network (Figure 1F). Furthermore, FRCs ensheathing CD31$^+$ high endothelial venules (HEVs) were transgene-positive (Figure 1G). *Ccl19-cre*$^+$ LN FRCs expressed CCL21 (Figure 1H, arrows) and CCL19 (Figure 1I, arrows) indicating that the *Ccl19-cre* transgene targets both past and present CCL19 expression in these nonhematopoietic cells.

Stromal cell composition in spleen is different from LNs because the double-negative (DN, PDPN$^-$CD31$^-$) fraction is dominant and PDPN$^+$CD31$^+$ LECs are not present in this organ (Onder et al., 2011). *Ccl19-cre* transgene activity was highest in the DN cell population (Figures S1C and S1D) with EYFP$^+$ cells being dispersed in all compartments of the white pulp (Figure S1E). High densities of transgene-positive cells could be detected in the area of the marginal zone (Figure S1F) and around central arterioles (Figure S1G). In contrast, transgene activity in PP stromal cells was high in PDPN$^+$CD31$^-$ cells and moderate in DN cells with around 80% and 20% of all EYFP$^+$ cells, respectively (Figures S1H and S1I). Because PDPN$^+$ CD31$^-$ cells in PPs are still undefined, we have referred to them as FRC-like cells. Transgene-positive cells were rare in subdomal areas and more dense in the abluminal part of the PP (Figure S1J), but associated both with T cell- and B cell-rich areas (Figure S1K), suggesting that PP FRC-like cells are involved in the orchestration of both T and B cell responses. Taken together, the *Ccl19-cre* transgene permits in vivo targeting of LN FRCs and FRC-like cells of PPs.

LN Formation Is Independent of LTβR-Signaling in *Ccl19-Cre*$^+$ Mesenchymal Stromal Cells

To assess *Ccl19-Cre* transgene activity during early LN development, we determined reporter gene expression in inguinal LN anlagen of *Ccl19-cre* × *R26-eyfp* on E16.5 and E18.5. We found that *Ccl19-cre*$^+$ stromal cells were highly abundant in the E16.5 inguinal LN anlage (Figures 2A; Figure S2A). Furthermore, the E16.5 inguinal LN anlage had attracted CD4$^+$ LTi cells, which most likely deliver the necessary LT$\alpha_1\beta_2$ for stimulation of the LTβR on mesenchymal stromal organizer cells. The number of *Ccl19-cre*$^+$ stromal cells grew approximately 3-fold until E18.5, whereas the CD4$^+$ LTi cell population expanded only modestly (Figure 2B; Figure S2B). To assess whether Cre-recombinase expression reflected the kinetics of *Ccl19* expression in developing LNs, we determined both Cre-recombinase and *Ccl19* mRNA production in neonatal and week 2 and six LN homogenates by quantitative RT-PCR (qRT-PCR). Endogenous *Ccl19* expression (Figure 2C) correlated well with Cre expression (Figure 2D) driven by the *Ccl19* promoter on the BAC transgene. In contrast, *Ltbr* expression fluctuated with the highest expression being measureable in the neonatal LN (Figure 2E). Confocal microscopic analysis revealed that *Ccl19-cre* transgene expression was highly abundant in neonatal inguinal LNs (Figure 2F, left panels). 3D reconstruction of high-resolution analyses indicated that *Ccl19-cre*-expressing stromal cells in the developing LN had formed a dense network (Figure 2F, right panels) reminiscent of the FRC network in the adult LN. Whereas *Ccl19-cre*$^+$ stromal cells expressed low amounts of PDPN, the mesenchymal markers smooth muscle actin (SMA) and platelet-derived growth factor receptor-β (PDGFRβ) were highly expressed (Figure 2G), indicating that the *Ccl19-cre* transgene targets mesenchymal stromal cells in developing LNs.

The differentiation of adult stromal cell subpopulations is thought to depend on LTβR signaling (Randall et al., 2008; van de Pavert and Mebius, 2010). Because lymphocytes are rare in neonatal LNs and LTβR-dependent stimulation of mesenchymal stromal cells is mainly provided by LTi cells (Cupedo et al., 2004b; White et al., 2007), it is most likely that *Ccl19-cre*$^+$ mesenchymal stromal cell in neonatal LNs received LTβR signals from LTi cells. Interestingly, deletion of the LTβR on *Ccl19-cre*$^+$ mesenchymal stromal cells did not abrogate LN formation (Figure 2H). Furthermore, formation of a stromal cell network in neonatal LNs was not affected by mesenchymal stromal cell-specific LTβR-ablation (Figure 2H, right panels). Likewise, expression of SMA and PDGFRβ (Figure 2I) was not altered by the selective LTβR-ablation. Gross pathological examination of adult *Ccl19-cre* × *Ltbr*$^{fl/fl}$ mice (4–6 weeks) after injection of Evan's Blue revealed that all LNs were present (data not shown). In contrast, *Ccl19-cre*-dependent ablation of the LTβR in PPs led to significantly reduced PP numbers (Figure S2C). Taken together, these data indicate that *Ccl19-cre* expression in PP mesenchymal stromal cells occurs in a developmental window of critical LTβR-sensitivity. Conversely, *Ccl19-cre*-expressing mesenchymal stromal cells in developing LNs do not require LTβR signals to facilitate LN formation.

LN Structure and Organization in the Absence of FRC-Specific LTβR Signaling

To assess the impact of *Ccl19-cre*-mediated LTβR-ablation on global LN structure and organization, we utilized recently developed optical projection tomography (OPT) routines (Kumar et al., 2010). The mesoscopic imaging analysis revealed that LNs of *Ccl19-cre* × *Ltbr*$^{fl/fl}$ mice had developed clearly distinguishable B cell follicles and a HEV network (Figure 3A). Quantification of the 3D data showed that conditionally LTβR-deficient LNs were approximately 25%–30% smaller than control LNs (Figure 3B) and exhibited a comparable reduction in B cell follicle size (Figure 3C), HEV length (Figure 3D), and complexity of the HEV network (Figure 3E). The OPT-based finding that LNs with FRC-specific LTβR-deficiency were still able to establish the basic LN infrastructure was supported by confocal microscopy, which showed that LNs had generated clearly distinguishable T and B cell zones (Figure 3F). The global reduction of LN size without specific impairment of substructures was reflected by the comparable reduction of various hematopoietic cell populations (Figure 3G). Thus, FRC-specific ablation of LTβR-signaling did not affect the formation of the basic LN structure with clear T and B cell zone segregation.

To assess whether the conditional LTβR-deficiency affects LN stromal cell composition, we prepared single-cell suspensions from *Ccl19-cre* × *Ltbr*$^{fl/fl}$ and control *Ltbr*$^{+/+}$ LNs, depleted CD45$^+$ hematopoietic cells and stained the enriched stromal cells with antibodies against PDPN and CD31. Flow cytometric analysis revealed a loss of PDPN$^+$CD31$^-$ cells that coincided with a significant increase of PDPN$^-$CD31$^-$ cells (Figure 4A).

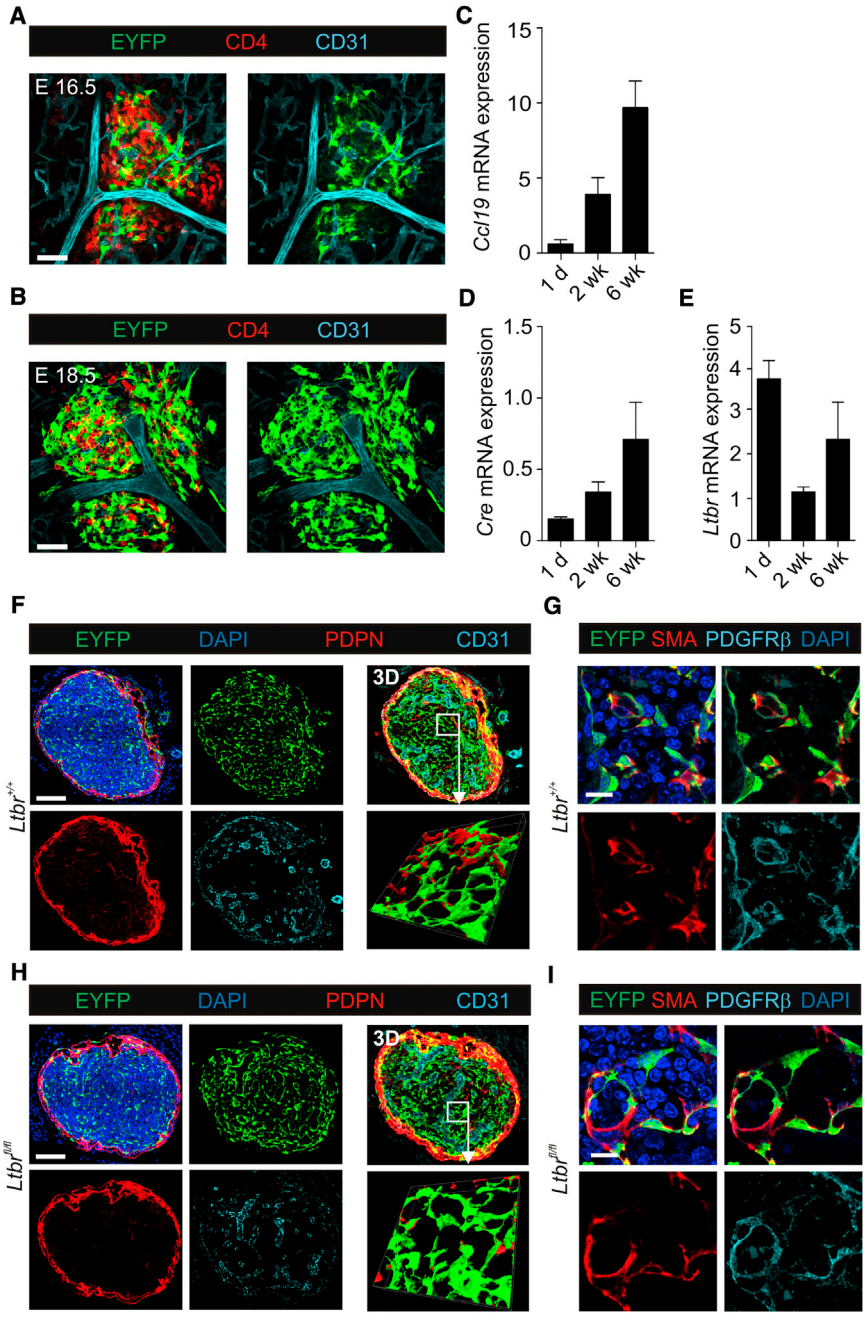

Figure 2. Characterization of *Ccl19-cre*$^{+}$ Mesenchymal Stromal Cells in Developing LNs

(A–E) *Ccl19-cre* × *R26-eyfp* embryos were analyzed for transgene expressing cells in inguinal LN anlagen by confocal microscopy at embryonic days E16.5 (A) and E18.5 (B) by using the indicated stainings. Left panels show merge of all channels; scale bars represent 100 μm. Inguinal LNs from neonatal, 2- and 6-week-old *Ccl19-cre* mice were analyzed by quantitative RT-PCR for the expression of *Ccl19* (C), Cre recombinase (D), and *Ltbr* (E). Values indicate mean ± SEM from two individual LNs from three mice analyzed in two independent experiments.

(F) Confocal microscopic analysis with single and combined stainings for the indicated markers of neonatal inguinal LNs from *Ccl19-cre* × *R26-eyfp* mice (confocal plane in left panels). Maximum intensity projection (3D) from z stack (upper right panel) and magnified 3D rendering of fibroblastic network (lower right panel, represents boxed area in upper panel); scale bars represent 100 μm.

(G) Expression of the smooth muscle actin (SMA) and platelet-derived growth factor receptor-β (PDGFRβ) in neonatal inguinal LNs from *Ccl19-cre* × *R26-eyfp* mice; scale bar represents 10 μm.

(H) Neonatal inguinal LNs from conditionally LTβR-deficient *Ccl19-cre* × *R26-eyfp* mice analyzed by confocal microscopy (confocal plane in left panels) with maximum intensity projection (3D) from z stack (upper right panel) and magnified 3D rendering of fibroblastic network (lower right panel, represents boxed area in upper panel); scale bars represent 100 μm.

(I) Expression of SMA and PDGFRβ in conditionally LTβR-deficient neonatal inguinal LNs; scale bar represents 10 μm. Representative data from one out of three independent experiments. See also Figure S2.

Importantly, the remaining PDPN^{+}CD31^{-} cells had lost LTβR expression (Figures 4B and 4C). Confocal microscopic analysis confirmed the substantial reduction of PDPN expression in *Ccl19-cre* × *Ltbr*$^{fl/fl}$ LNs (Figure 4D). However, ERTR7 protein production and the formation of the fibroblastic reticular network was not affected by FRC-specific LTβR ablation (Figure 4D). Moreover, the fibroblastic network still generated ERTR7-ensheathed collagen bundles (Figure 4E), i.e., the conduit system, which rapidly drained small molecules through the T cell zone, both in the presence and absence of LTβR on T cell zone reticular cells (Figure 4F). T cell zone reticular cells both in the LN parenchyma and surrounding HEVs had lost CCL21 positivity in *Ccl19-cre* × *Ltbr*$^{fl/fl}$ LNs, whereas vascular endothelial cells in HEVs still produced this chemokine (Figure 4G). Quantitative RT-PCR analysis of whole LN homogenates confirmed the substantial loss of *Ccl21* mRNA expression in conditionally LTβR-deficient LNs (Figure 4H). Moreover, *Ccl19-cre* × *Ltbr*$^{fl/fl}$ LNs produced significantly less *Ccl19* (Figure 4I) and *Il7* (Figure 4J) mRNA but almost normal amounts of the B cell zone chemokine *Cxcl13* (Figure 4K). Taken together, these data show that *Ccl19* promoter-dependent LTβR-ablation profoundly altered the LN stromal cell composition and abolished expression of molecules in T cell zone reticular cells, which are considered part of the molecular signature of FRCs.

LTβR Promotes FRC Differentiation from Myofibroblastic Precursors

The pronounced reduction of PDPN^{+} FRCs and the concomitant increase in DN stromal cells in LNs *Ccl19-cre* × *Ltbr*$^{fl/fl}$ suggested that DN LN stromal cells may differentiate into FRCs.

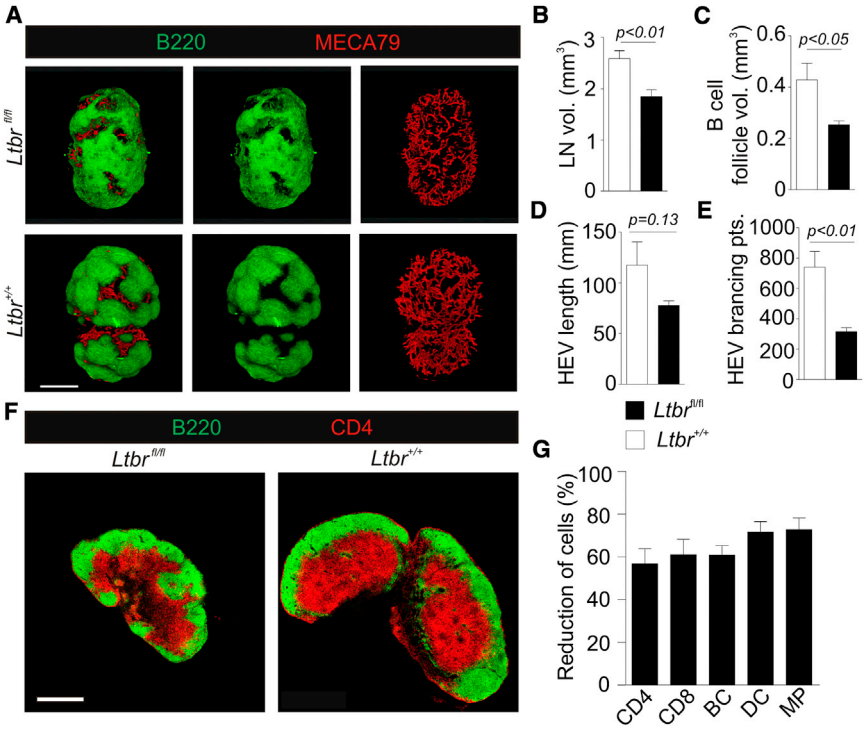

Figure 3. Impact of FRC-Specific LTβR Signaling on Peripheral LN Structure

(A) Inguinal LNs from 4-week-old *Ccl19-cre* × *Ltbr*$^{fl/fl}$ and *Ltbr*$^{+/+}$ controls were analyzed by OPT for the presence of the HEV network (MECA-79^{+}) and B cell follicles (B220^{+}); scale bar represents 500 μm. Quantitative analysis based on OPT data for (B) LN volume, (C) B cell follicle volume, (D) HEV network length, and (E) HEV branching points (mean ± SEM, n = 6 mice pooled from two independent experiments).

(F) Confocal microscopic analysis of inguinal LNs from 4-week-old *Ccl19-cre* × *Ltbr*$^{fl/fl}$ and *Ltbr*$^{+/+}$ controls by using antibodies against T cells (CD4) and B cells (B220); scale bar represents 200 μm.

(G) Flow cytometry-based quantification of LN cellularity. Values indicate relative cell numbers in *Ccl19-cre* × *Ltbr*$^{fl/fl}$ mice compared to *Ltbr*$^{+/+}$ mice (CD4, CD4^{+} T cells; CD8, CD8^{+} T cells; BC, B cells; DC, dendritic cells; MP, macrophages; mean ± SEM, n = 6 mice from two independent experiments).

Indeed, in vitro culture of sorted DN cells from *Ccl19-cre* × *R26-eyfp* LNs in the presence of LTi cells resulted in activation of the *Ccl19* promoter (Figures S3A–S3C). Moreover, upregulation of EYFP was accompanied by a pronounced increase in PDPN expression (Figure S3D). Crossing of *Ccl19-cre* × *Ltbr*$^{fl/fl}$ mice with *R26-eyfp* reporter mice confirmed that genetically labeled (i.e., EYFP^{+}) FRCs emerge from DN precursors in a LTβR gene dose-dependent fashion (Figures 5A and 5B). LTβR-dependent FRC maturation was associated not only with the upregulation of PDPN (Figure 5A) but also with a substantial increase in ICAM-1 and VCAM-1 expression (Figure 5C). Likewise, EYFP^{+} PDPN^{lo} cells from *Ccl19-cre* × *R26-eyfp* LNs expressed moderate amounts of ICAM-1 and VCAM-1 (Figure S3E). To further characterize the phenotypical changes associated with LTβR-dependent FRC differentiation, we first determined the expression of myofibroblast and pericyte markers in LN stromal cell preparations. As shown in Figure 5D, abortion of FRC maturation was associated with increased *Acta2*, *Cnn1*, and *Pdgfrb* mRNA expression, whereas *Pdgfra* and *Cspg4* mRNA expression was not affected. Confocal microscopy confirmed upregulation of SMA in myofibroblastic FRC precursors surrounding HEVs (Figure 5E) and in the T cell zone network (Figure 5F, arrowheads). Likewise, PDGFRβ was upregulated in FRC precursors in both locations (Figure 5G), whereas perivascularly expressed calponin-1 was specifically upregulated in myofibroblastic cells in the T cell zone network (Figure 5H). In contrast, the expression of the pericyte marker NG2 around small blood vessels was not affected by the selective LTβR-deficiency (Figure 5I). Thus, myofibroblastic FRC precursors require LTβR stimulation to acquire the characteristic mature phenotype with the expression of homeostatic and immune-regulatory molecules.

FRC Maturation Guarantees Immunocompetence during Viral Infection

To determine the functional consequences of FRC-specific LTβR-deficiency on intranodal T cell migration, we utilized intravital 2-photon microscopy. Adoptive transfer of C57BL/6 T cells into *Ccl19-cre* × *Ltbr*$^{fl/fl}$ mice or control mice revealed a significant reduction of T cell speed in the T cell zone parenchyma under conditions of selective LTβR-ablation, with an average speed close to *Ccr7*$^{-/-}$ T cells (Figure 6A). In contrast, T cell speed around HEVs was not affected by the absence of mature FRCs (Figure 6A). Because T cell motility within the T cell zone parenchyma is partially dependent on CCR7-mediated signals (Worbs et al., 2007; Figure 6A), we assessed whether LTβR-dependent FRC maturation with upregulation of CCR7 ligands impacts on dendritic cell (DC)-CD8^{+} T cell interaction. To this end, mouse hepatitis virus (MHV)-specific CD8^{+} T cells expressing a T cell receptor recognizing the H2-K^{b}-binding S598 epitope were adoptively transferred into *Ccl19-cre* × *Ltbr*$^{fl/fl}$ or LTβR-competent control mice. Subsequent subcutaneous injection of S598-pulsed DCs revealed that the conditional LTβR ablation did not lead to a reduction of DC-mediated T cell activation (Figures S4A and S4B). Next, we assessed whether the conditional LTβR-deficiency affects global immune responsiveness in *Ccl19-cre* × *Ltbr*$^{fl/fl}$ mice by using systemic infection with the lymphocytic choriomeningitis virus (LCMV) WE strain, which is controlled in a CD8^{+} T cell and perforin-dependent manner (Kägi et al., 1994). Conditionally LTβR-deficient mice failed to reduce viral titers in LNs and to clear the virus from peripheral organs such as the kidney by day 8 postinfection (Figure S4C). Furthermore, *Ccl19-cre* × *Ltbr*$^{fl/fl}$ mice showed significantly reduced antiviral T cell responses in LNs (Figure S4D), indicating a globally reduced capacity to cope with viral infections when LN FRCs fail to generate an immune-stimulatory environment. However, under conditions of systemic LCMV distribution, other factors than deficient LN

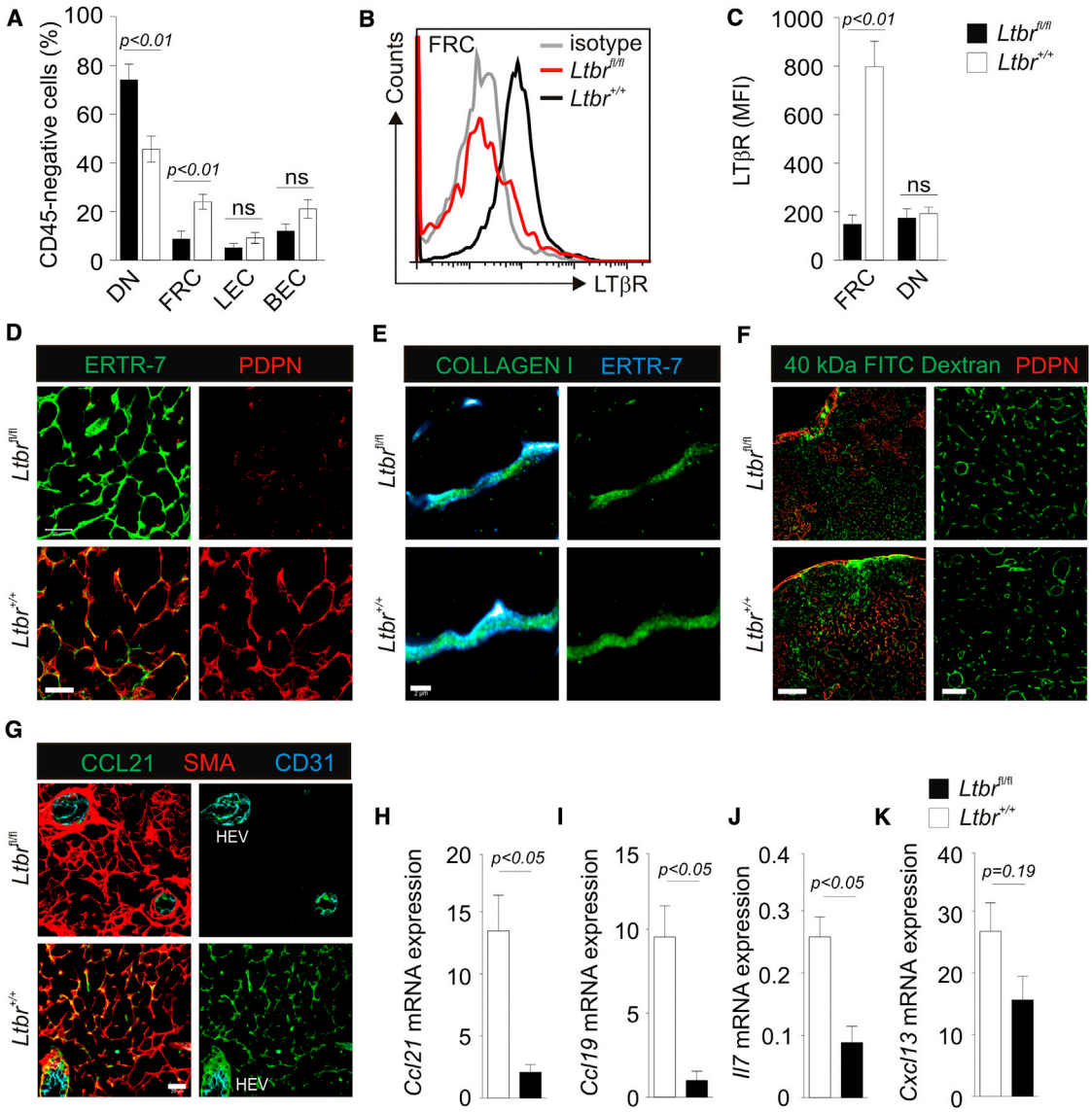

Figure 4. FRC-Specific LTβR Ablation Alters LN Stromal Cell Composition and Phenotype

(A) Frequency of the major stromal cell populations (PDPN$^-$CD31$^-$ DN cells, PDPN$^+$CD31$^+$ [FRC], PDPN$^+$CD31$^+$ [LEC]; PDPN$^-$CD31$^+$ [BEC]) in inguinal LNs from *Ccl19-cre* × *Ltbr*$^{fl/fl}$ and *Ltbr*$^{+/+}$ mice as determined by flow cytometry; values represent mean ± SEM (n = 9 mice from three independent experiments).

(B) Representative LTβR expression patterns on PDPN$^+$CD31$^-$ (FRC) stromal cells of *Ccl19-cre* × *Ltbr*$^{fl/fl}$ (red) and *Ltbr*$^{+/+}$ (black) mice determined by flow cytometry; staining with isotype control antibody in gray.

(C) Summary of LTβR expression displayed as mean fluorescent intensity (MFI), mean ± SEM (n = 4 mice from two independent experiments).

(D–G) Confocal microscopic analysis of inguinal LN stromal cells from 6-week-old *Ccl19-cre* × *Ltbr*$^{fl/fl}$ and *Ltbr*$^{+/+}$ controls. (D) T cell zone reticular network revealed by ERTR-7 and PDPN staining, merged channels in left panel; scale bar represents 20 μm. (E) High-resolution analysis of T cell zone conduit with collagen-1 bundles ensheathed by ERTR-7; scale bar represents 2 μm. (F) Drainage of 40 kDa FITC dextran through LN conduits 2 min after subcutaneous injection. Left panel shows magnified FITC staining in T cell zone; scale bar represents 100/40 μm. (G) Vascular (HEV, high endothelial venule) and T cell zone stromal cell-associated CCL21 expression, merged channels in left panel, CD31 and CCL21 merge in right panel; scale bar represents 20 μm.

(H–K) Inguinal LNs from 6-week-old *Ccl19-cre* × *Ltbr*$^{fl/fl}$ and *Ltbr*$^{+/+}$ controls were analyzed by quantitative RT-PCR for the expression of *Ccl21* (H), *Ccl19* (I), *Il7* (J), and *Cxcl13* (K). Values indicate mean ± SEM from two individual LNs from three mice analyzed in two independent experiments.

FRC maturation, such as the lack of PPs, could have contributed to the observed immunodeficiency in *Ccl19-cre* × *Ltbr*$^{fl/fl}$ mice. Therefore, we resorted to an infection system with exclusive replication in a tissue-draining LN. Following intranasal application, the murine coronavirus MHV establishes an infection in the central nervous system (CNS) during which systemic spread is prevented by swift induction of antiviral immune responses in the cervical LN (Cervantes-Barragán et al., 2009; Gil-Cruz et al., 2012). Successful control of the acute MHV infection depends on type I interferon (IFN)-producing plasmacytoid

dendritic cells (Cervantes-Barragan et al., 2012b) and both $CD8^+$ and $CD4^+$ T cells (Bergmann et al., 2006). To assess the impact of the relative deficiency of CCR7 ligands in LN stromal cells of *Ccl19-cre* × $Ltbr^{fl/fl}$ mice, we compared conditionally LTβR-deficient mice with *plt/plt* mice, which lack the expression of CCR7 ligands specifically in secondary lymphoid organs (Gunn et al., 1999). We found that mice with FRC-specific LTβR deficiency showed a more dramatic weight loss compared to *plt/plt* mice (Figure 6B) and exhibited higher viral titers in the CNS at day 10 postinfection (Figure 6C). The failure of both *Ccl19-cre* × $Ltbr^{fl/fl}$ and *plt/plt* mice to clear the virus from the CNS and hence to prevent weight loss is most likely due to the strongly impaired antiviral T cell response in this vulnerable organ (Figure 6D). Interestingly, recruitment of fully activated IFN-γ-secreting effector T cells (Figures 6E and 6F) was reduced in *Ccl19-cre* × $Ltbr^{fl/fl}$ compared to *plt/plt* mice indicating that the impaired antiviral immunity in *Ccl19-cre* × $Ltbr^{fl/fl}$ mice can only be partially explained by the lack of CCL19 and CCL21 within the CNS-draining LN. Taken together, these data indicate that LTβR-mediated maturation of LN FRCs is critical for the generation of protective antiviral T cell responses.

DISCUSSION

The assembly of hematopoietic LTi cells and mesenchymal stromal cells in the LN anlage and their positive feedback-type interaction is one of the first critical steps in LN formation. Whereas the molecular details involved in LTi cell-dependent stimulation of LN development have been thoroughly described (reviewed in Randall et al., 2008; van de Pavert and Mebius, 2010), the characterization of the stromal side of the LTi-mesenchymal LTo cell interaction has suffered from the lack of suitable tools to dissect ontogeny and function of these cells. We have addressed this need and describe in this study a model based on cell-specific expression of the Cre-recombinase that facilitates the dissection of mesenchymal stromal cell development during LN formation and the definition of critical molecular interactions between mesenchymal stromal and hematopoietic cells.

Mesenchymal precursors in the LN anlage express PDPN, but are ICAM-1- and VCAM-1-negative (Cupedo et al., 2004a; White et al., 2007; Bénézech et al., 2010). These precursors develop into the mesenchymal LTo cell defined by intermediate to high ICAM-1 and VCAM-1 expression and the concomitant upregulation of essential molecules involved in LN organogenesis, including CCL19 (Bénézech et al., 2010) Notably, LTβR and the tumor necrosis factor receptor 1 (TNFR1) are highly expressed on both the mesenchymal precursor and the mesenchymal LTo cell (Bénézech et al., 2010) whereby LTβR signaling in the mesenchymal precursor is critical for the transition to the ICAM-1^+VCAM-1^+ mesenchymal LTo cells (White et al., 2007). However, ablation of LTβR signaling in mesenchymal stromal cells in the developing LN, i.e., ICAM-1^+VCAM-1^+ stromal cells expressing CCL19 in our model, did not prohibit the formation of LNs and the transition of the mesenchymal stromal cells of the prenatal LN into myofibroblastic FRC precursors (pre-FRCs) in postnatal LNs. Importantly, progression toward the immune-stimulatory, mature FRC was strictly dependent on LTβR signaling. Thus, our data together with previous studies (White et al., 2007; Bénézech et al., 2010) indicate that LN mesenchymal stromal cell development is characterized by two distinct developmental windows of critical LTβR signaling, i.e., initially during the transition of the mesenchymal precursor to the mesenchymal LTo cells and as a final maturation stimulus for T cell zone FRCs.

Development of PPs starts with recruitment of hematopoietic LTi cells and CD11c-expressing lymphoid tissue initiator cells (Yoshida et al., 1999; Veiga-Fernandes et al., 2007), which both serve as sources of LTβR ligands. Again, LTβR-mediated stimulation of mesenchymal LTo cells triggers production of homeostatic cytokines and IL-7, which are essential for PP development (Adachi et al., 1998; Finke et al., 2002). The results of our study indicate that CCL19 expression in developing PP mesenchymal stromal cells occurs during a critical phase of LTβR sensitivity. In contrast, LTβR signaling in *Ccl19-Cre*$^+$ mesenchymal stromal cells in LN anlagen was not mandatory for LN development. However, the presence of the LTβR on endothelial cells appears to be essential during early stages of LN formation (Onder et al., 2013). Future studies utilizing the *Ccl19-Cre* model and other stromal cell-specific Cre-driver mice will provide a comprehensive characterization of the critical LTβR-sensitive stage during LTo development in LNs and PPs.

Several functions have been assigned to FRCs in adult LNs, such as the generation of the conduit system to facilitate rapid transfer of small antigens through the T cell zone (Sixt et al., 2005), regulation of the LN vasculature (Chyou et al., 2008), coordination of T cell and dendritic cell interaction (Bajénoff et al., 2006), maintenance of T cell homeostasis via IL-7 (Link et al., 2007), and tolerization of self-reactive T cells (Fletcher et al., 2010). Our analysis indicates that the basic infrastructure of the LN including the conduit system and the HEV network is generated by myofibroblastic FRC-precursors in an LTβR-independent fashion. It remains to be determined whether other receptors involved in lymphoid organogenesis such as RANKL or TNFR1 compensate for the lack of LTβR. Clearly, LTβR-signaling was necessary for the maturation of FRCs from PDPN-negative myofibroblastic precursors and the optimal support of antiviral immunity provided by the adaptive immune system. Following exposure to inflammatory stimuli, FRCs respond with an activation program that leads to upregulation of molecules involved in innate and adaptive immune responses (Vega et al., 2006; Malhotra et al., 2012). Hence, it is likely the LTβR-mediated stimulation of pre-FRCs serves as a critical switch for global immune responsiveness by unleashing the full immune-stimulatory capacity of the mature FRC.

In conclusion, our study provides further evidence for a common theme in mesenchymal stromal cell differentiation, namely the LTβR-dependent conversion of a sessile myofibroblast into an immunologically highly active stromal cell. Such profound LTβR-mediated transformation into FRC-like cells has been described for vascular smooth-muscle cells during the formation of organized lymphoid follicles surrounding heavily atherosclerotic aortas (Lötzer et al., 2010). Likewise, follicular dendritic cells (FDCs) that develop in ectopic lymphoid tissues can descend from PDGFRβ-expressing perivascular precursors (Krautler et al., 2012). Interestingly, only the final maturation of

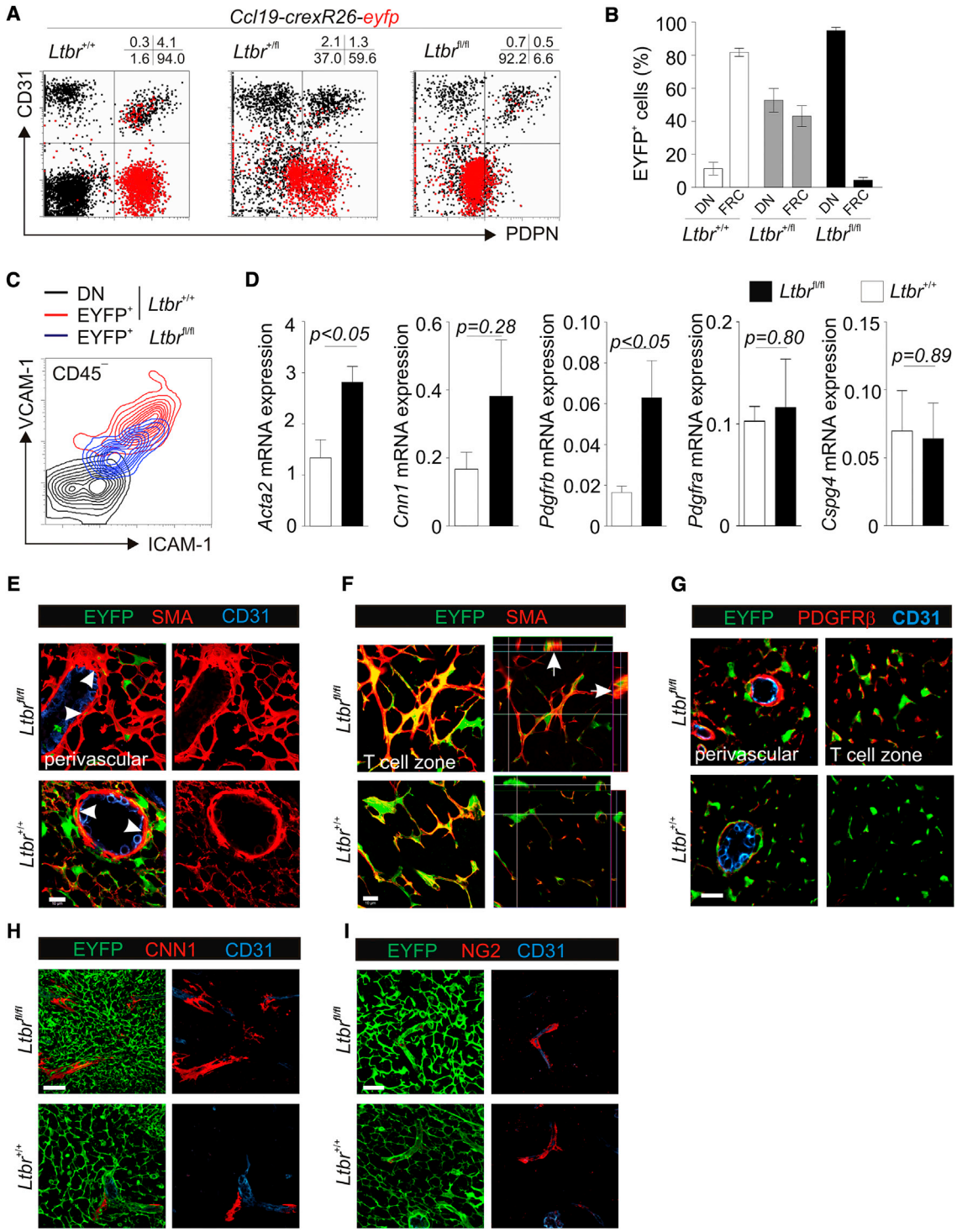

Figure 5. LTβR-Dependent FRC Maturation

(A) LN stromal cells from 6-week-old *Ccl19-cre* × *R26-eyfp* mice with wild-type ($^{+/+}$, WT) and heterozygously ($^{+/fl}$) or homozygously floxed ($^{fl/fl}$) *Ltbr* loci were assessed by flow cytometry for EYFP expression by using back gating. Representative dot plot analysis with quadstat values of CD31 and PDPN expression is shown.

(B) EYFP expression in FRCs and DN cells in the indicated *Ltbr* genotype of *Ccl19-cre* × *R26-eyfp* mice; mean ± SEM (n = 3 mice from two independent experiments).

(C) Representative analysis of ICAM-1 and VCAM-1 expression on *Ltbr*$^{+/+}$ DN cells from *Ccl19-cre* × *R26-eyfp* mice (black), EYFP^{+} *Ltbr*$^{+/+}$ FRCs of *Ccl19-cre* × *R26-eyfp* mice (red), and EYFP^{+} cells of *Ccl19-cre* × *R26-eyfp*x*Ltbr*$^{fl/fl}$ mice (blue).

(D) Inguinal LNs from 6-week-old *Ccl19-cre* × *Ltbr*$^{fl/fl}$ and *Ltbr*$^{+/+}$ controls were analyzed by quantitative RT-PCR for the expression of *Acta2* (SMA), *Cnn1* (Calponin-1), *Pdgfrb*, *Pdgfra*, and *Cspg4* (NG2). Values indicate mean ± SEM from two individual LNs from >3 mice analyzed in two independent experiments.

(legend continued on next page)

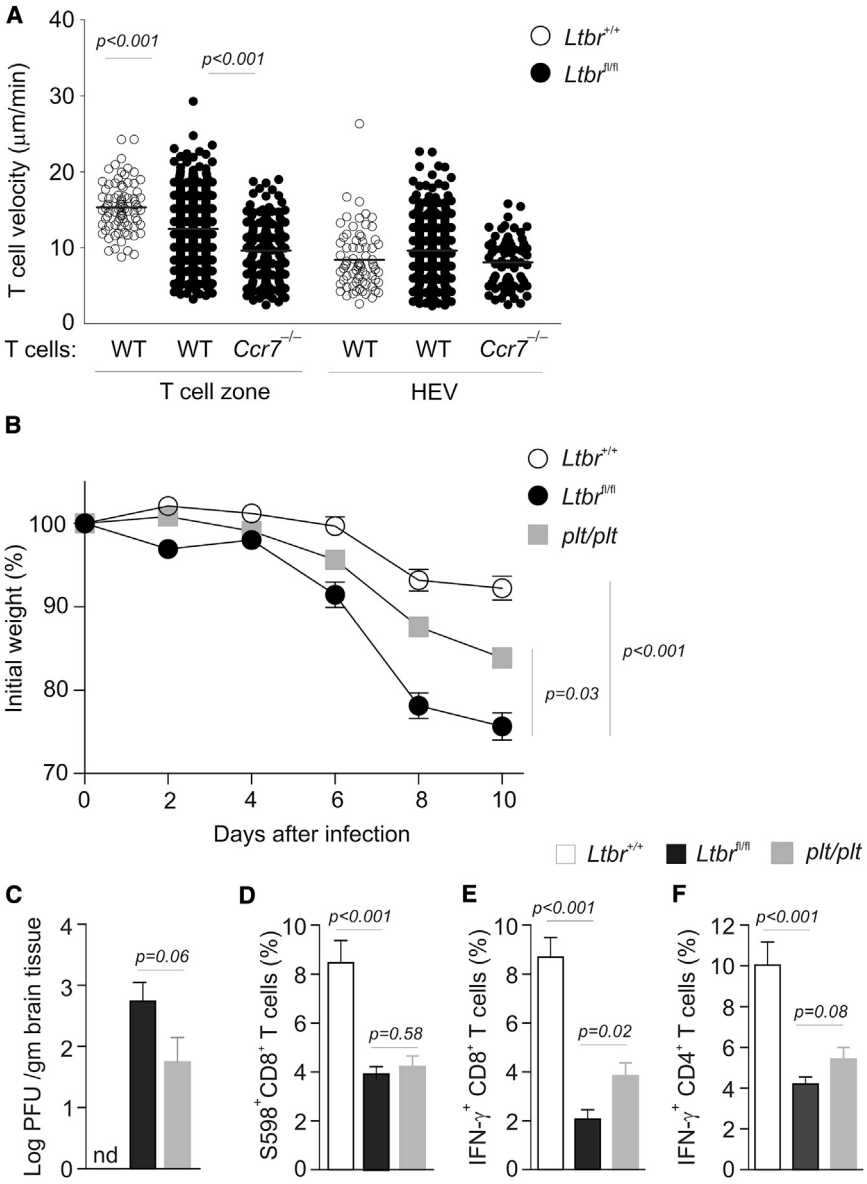

Figure 6. T Cell Function in the Absence of FRC-Specific LTβR Signaling

(A) Motility of T cells from C57BL/6N (WT) or CCR7-deficient donors in the T cell zone and around HEVs in popliteal LNs of *Ccl19-cre* × $Ltbr^{fl/fl}$ (closed symbols) and $Ltbr^{+/+}$ (open symbols) mice as determined by intravital two-photon microscopy. Values represent single tracks pooled from two independent experiments (n = 4 mice, mean indicated by horizontal bar).

(B–D) *Ccl19-cre* × $Ltbr^{fl/fl}$, $Ltbr^{+/+}$, and *plt/plt* mice were infected intranasally with 5 × 10^4 pfu of MHV A59. (B) Weight loss was recorded during the indicated time period following infection. Values indicate mean percentage of the initial weight ± SEM (n = 8 mice per group, one-way ANOVA with Tukey's post test). (C) Viral titers in brain homogenates were determined at day 10 postinfection. Data represent mean viral titers ± SEM, pooled data from two independent experiments (n = 8 mice); nd, not detectable. (D) T cell responses were determined by tetramer analysis of CNS-infiltrating S598-specific $CD8^+$ T cells (left panel) and intracellular staining for S598-responsive IFN-γ-producing $CD8^+$ T cells (middle panel), and M133-responsive IFN-γ-producing $CD4^+$ T cells (right panel) on day 10 post infection. Values indicate mean percentages ± SEM of specific cells in the respective $CD8^+$ or $CD4^+$ T cell population (n = 8 mice per group). See also Figure S4.

(D–F) T cell responses were determined by tetramer analysis of CNS-infiltrating S598-specific $CD8^+$ T cells (D) and intracellular staining for S598-responsive IFN-γ-producing $CD8^+$ T cells (E), and M133-responsive IFN-γ-producing $CD4^+$ T cells (F) on day 10 postinfection. Values indicate mean percentages ±SEM of specific cells in the respective $CD8^+$ or $CD4^+$ T cell population (n = 8 mice per group).

FDCs into immunologically active cells was dependent on lymphotoxin-mediated signals. Whereas FDCs in ectopic lymphoid tissues can emerge from ubiquitous perivascular precursors (Krautler et al., 2012), mature LN FRCs originate from PDPN-negative myofibroblastic progenitors that can form the global stromal cell network of the developing LN and that are distributed throughout the T cell zone and interfollicular regions of the adult LN. Despite the remaining unknowns concerning the differentiation of mesenchymal stromal cells of secondary and tertiary lymphoid organs, the results of this study suggest that timing of LTβR targeting for the attenuation of exaggerated immune responses may be critical (Browning, 2008), i.e., mesenchymal stromal cell differentiation should be blocked before the stage of the immunologically fully active FRC—or FDC—has been reached.

EXPERIMENTAL PROCEDURES

Mice

BAC-transgenic C57BL/6N-*Tg(Ccl19-Cre)*^{489Biat} (*Ccl19-Cre*) mice were generated as described previously (Onder et al., 2011). The coding sequence for the Cre-recombinase and a truncated form of the human *CD4* gene, separated by an IRES sequence and including a stop codon, was inserted into *Ccl19* exon 1 utilizing the endogenous ATG translation start codon on the 180 kb BAC RP23

(E–I) Confocal microscopic analysis of inguinal LN stromal cells from 6-week-old *Ccl19-cre* × *R26-eyfp*x$Ltbr^{fl/fl}$ mice and $Ltbr^{+/+}$ *Ccl19-cre* × *R26-eyfp* controls. Reconstruction of perivascular (E) and T cell zonal (F) stromal cell network by analyzing CD31, SMA, and EYFP expression is shown. Arrowheads indicate perivascular EYFP expression, arrows indicate SMA^+EYFP^+ cells in orthogonal sections, and scale bars represent 10 μm.

(G) Analysis of perivascular and T cell zonal expression of EYFP and PDGFRβ; scale bar represents 20 μm, all panels show merged channels. Reconstruction of perivascular and network-forming cells expressing CNN1 (H) and NG2 (I) and EYFP, merged channels in left panels; scale bars represent 30 μm; representative data out of three independent experiments. See also Figure S3.

446D10 (Invitrogen). Because the *Ccl21b* gene is in close proximity to *Ccl19*, the *Ccl21b* gene was deleted on the BAC by inserting the human *CD8* gene into the first exon of the *Ccl21b* locus. The BAC carried at least 90 kb of sequence upstream of the *Ccl19* transcription start site. Integration of the Cre-recombinase was confirmed by Southern blot analysis. Modified BACs were screened with 5′ATG PCR (forward 5′-GCACACGAATGTGGATGTTC-3′, reverse 5′-CTGCACACAGACAGGAGCAT-3′) and 3′polyA PCR (forward 5′-ATGTGGCAGTGTCTGCTGAG-3′, reverse 5′-CCTGTAGCCAGAGGTTG GAG-3′). Founder lines were genotyped by PCR by using the following primers: forward 5′-TCTCTGCCCAGAGTCATCCT-3′, reverse 5′-ATGC TCCTGTCTGTGTGCAG-3′. B6.129X1-Gt(ROSA)26Sor^{tm1Hjf} (*R26-eyfp*) mice were purchased from The Jackson Laboratories. *Ltbr*$^{fl/fl}$ mice (Wimmer et al., 2012) were described previously. C57BL/6N mice were obtained from Charles River (Sulzfeld, Germany) and *plt*/*plt* mice were obtained from the Institute of Laboratory Animal Sciences (University of Zurich, Switzerland). All animals were kept under conventional conditions in individually ventilated cages. Experiments were performed in accordance with Swiss federal and cantonal guidelines (Tierschutzgesetz) under the permission numbers SG11/05 and SG11/04 granted by the Veterinary Office of the Canton of St. Gallen.

Preparation of Stromal Cells

LNs were dissected into small pieces and transferred into a 24-well dish filled with RPMI 1640 medium containing 2% FCS, 20 mM HEPES (all from Lonza), 1 mg/ml Collagenase Type IV (Sigma), and 25 μg/ml DNaseI (Applichem). Dissociated LNs were incubated at 37°C for 30 min. After enzymatic digestion, cell suspensions were washed with PBS containing 0.5% FCS and 10 mM EDTA. To enrich the stromal cell fraction, hematopoietic cells were depleted by incubating the cell suspension with MACS anti-CD45 Microbeads and passing over a MACS LS column (Miltenyi).

Flow Cytometry and Cell Sorting

Single-cell suspensions were incubated for 20 min at 4°C in PBS containing 1% FCS and 10 mM EDTA with the following fluorescently labeled antibodies: anti-CD45, anti-PDPN, anti-CD31, anti-LTβR, anti-VCAM-1, and anti-ICAM-1 (all from eBioscience), anti-CD3, anti-CD4, anti-CD8, anti-B220, anti-CD11c, anti-CD11b, anti-F4/80 (all from BD Biosciences). Cells were acquired with a FACS Canto (BD Biosciences) and analyzed by using FlowJo software (Treestar). Cell sorting was performed by using a FACS Aria cell sorter (BD Biosciences).

Quantitative Real-Time PCR

Total cellular RNA was extracted from homogenized tissues and sorted cells by using TRIZOL reagent (Invitrogen) following the manufacturers' protocol. cDNA was prepared by using cDNA archive kit (Applied Biosystems) and quantitative RT-PCR was performed by using the Light Cycler-FastStart DNA Master SYBR Green I kit (Roche Diagnostics) on a LightCycler machine (Roche Diagnostics). mRNA expression was measured by using the following primers: *Ccl19* forward CTGCCTCAGATTATCTGCCAT, reverse AGGTAGCG GAAGGCTTTCAC; *Ccl21* forward AAGGCAGTGATGGAGGGG, reverse CGGGGTAAGAACAGGATTG; *tata-box binding protein* (tbp) forward CCTTCACCAATGACTCCTATGAC, reverse CAAGTTTACAGCCAAGATTCAC; *Cxcl13* forward ACAGCAACGCTGCTTCTCC, reverse AATCACTCCAGAA CACCTAC; *cre* forward ATGCTCCTGTCTGTGTGCAG, reverse GGAGGGCA GATCTCCTGTG; *Acta2* (QuantiTect Primer Assay QT00140119, QIAGEN); *cspg4* (QuantiTect Primer Assay QT00143220); *Cnn1* (QuantiTect Primer Assay QT00105420); P*dgfra* (QuantiTect Primer Assay QT00140021); *Pdgfrb* (QuantiTect Primer Assay QT00113148).

Immunohistochemistry

Lymph nodes were fixed overnight in freshly prepared 4% paraformaldehyde (Merck) at 4°C under agitation. Fixed LNs were embedded in 4% low melting agarose (Invitrogen) in PBS and sectioned with a vibratome (Leica VT-1200). We blocked 20–30 μm thick sections in PBS containing 10% FCS, 1 mg/ml anti-Fcγ receptor (BD Biosciences), and 0.1% Triton X-100 (Sigma). Sections were incubated overnight at 4°C with the following antibodies: anti-PDPN, anti-B220, anti-CD31, anti-CD4, anti-PDGFRβ, anti-LyveI, anti-E-Cadherin (all from eBioscience), anti-NG2 (Millipore), anti-SMA (Sigma), anti-EYFP (Clontech), anti-Calponin1, anti-CCL21, anti-CCL19, anti-Collagen I, anti-ERTR-7 (all from Abcam). Unconjugated antibodies were detected with the following secondary antibodies: Dylight649-conjugated anti-rat-IgG, Alexa488-conjugated anti-rabbit-IgG, Dylight549-conjugated anti-syrian hamster-IgG, and Dylight549-conjugated Streptavidin (all purchased from Jackson Immunotools). Microscopical analysis was performed by using a confocal microscope (Zeiss LSM-710) and images were processed with ZEN 2010 software (Carl Zeiss, Inc.) and Imaris (Bitplane).

Injection of Soluble Tracers

Mice were injected with 50 μg of 40 kDa FITC-Dextran (Molecular Probes) into the footpad and sacrificed two minutes after injection. Popliteal and inguinal LNs were excised and prepared for immunohistochemistry.

Optical Projection Tomography (OPT)

Mice received an intravenous injection of fluorescently labeled MECA-79 (15 μg) to label the HEV network. After 15 min, mice were sacrificed, LNs were carefully excised, and surrounding tissue was removed under a stereomicroscope. Sample preparation and OPT was performed as previously described (Kumar et al., 2010).

Two-Photon Intravital Microscopy

Purified T cells were fluorescently labeled with 2.5 μM chloromethyl-benzoyl amino-tetramethylrhodamine (CMTMR) or CFSE for 15 min at 37°C. After washing, labeled T cells were injected intravenously into sex-matched mice, which were 24 hr later anesthetized and surgically prepared to expose the right popliteal lymph node. Two-photon microscopy (2PM) was performed as described (Soriano et al., 2011).

Virus Infections

Mice were infected intranasally with 5×10^4 pfu of MHV A59 as previously described (Cervantes-Barragán et al., 2009). MHV titers were determined by standard plaque assay by using L929 cells. Analysis of MHV-specific CD8 T cell responses was performed by using PE-conjugated MHV S598/H-2K^b tetramers (Sanquin, Amsterdam, The Netherlands) as described (Cervantes-Barragán et al., 2012a). For peptide-specific cytokine production, 10^6 lymphocyte-enriched CNS cells were restimulated with S598 or M133 peptides and IFN-γ secretion was determined by flow cytometry as described (Cervantes-Barragán et al., 2012a). LCMV infection and assessment of viral titers and antiviral T cell responses were done as described previously (Cervantes-Barragán et al., 2012b).

Statistical Analysis

2PM and OPT data were analyzed with Volocity (Perkin Elmer). All statistical analyses were performed with Prism 5.0 (Graphpad Software Inc.). Data were analyzed with the nonpaired Student's t test or as indicated in the figure legend. A p value of < 0.05 was considered as significant.

SUPPLEMENTAL INFORMATION

Supplemental Information includes four figures and can be found with this article online at http://dx.doi.org/10.1016/j.immuni.2013.03.012.

ACKNOWLEDGMENTS

We would like to thank Rita DeGiuli for technical support and Alexander Link for help with designing the cloning strategy. This study received financial support from the Swiss National Science Foundation (Sinergia 125447/1 to J.V.S. and B.L.), the Wilhelm Sander Stiftung (to B.L.), and from the Austrian Genome Research Programme GEN-AU II and III (to T.R.). B.L. designed the study and wrote the paper; L.O. performed research and wrote the paper; E.S., J.V.S., V.T., T.S., and T.H. analyzed and discussed data; R.D., T.R., C.G.-C., C.P.-S., J.C., and Q.C. performed research and discussed data.

Received: August 21, 2012
Accepted: March 29, 2013
Published: April 25, 2013

REFERENCES

Adachi, S., Yoshida, H., Honda, K., Maki, K., Saijo, K., Ikuta, K., Saito, T., and Nishikawa, S.I. (1998). Essential role of IL-7 receptor alpha in the formation of Peyer's patch anlage. Int. Immunol. *10*, 1–6.

Bajénoff, M., Egen, J.G., Koo, L.Y., Laugier, J.P., Brau, F., Glaichenhaus, N., and Germain, R.N. (2006). Stromal cell networks regulate lymphocyte entry, migration, and territoriality in lymph nodes. Immunity *25*, 989–1001.

Bénézech, C., White, A., Mader, E., Serre, K., Parnell, S., Pfeffer, K., Ware, C.F., Anderson, G., and Caamaño, J.H. (2010). Ontogeny of stromal organizer cells during lymph node development. J. Immunol. *184*, 4521–4530.

Bergmann, C.C., Lane, T.E., and Stohlman, S.A. (2006). Coronavirus infection of the central nervous system: host-virus stand-off. Nat. Rev. Microbiol. *4*, 121–132.

Boos, M.D., Yokota, Y., Eberl, G., and Kee, B.L. (2007). Mature natural killer cell and lymphoid tissue-inducing cell development requires Id2-mediated suppression of E protein activity. J. Exp. Med. *204*, 1119–1130.

Browning, J.L. (2008). Inhibition of the lymphotoxin pathway as a therapy for autoimmune disease. Immunol. Rev. *223*, 202–220.

Cervantes-Barragán, L., Kalinke, U., Züst, R., König, M., Reizis, B., López-Macías, C., Thiel, V., and Ludewig, B. (2009). Type I IFN-mediated protection of macrophages and dendritic cells secures control of murine coronavirus infection. J. Immunol. *182*, 1099–1106.

Cervantes-Barragán, L., Firner, S., Bechmann, I., Waisman, A., Lahl, K., Sparwasser, T., Thiel, V., and Ludewig, B. (2012a). Regulatory T cells selectively preserve immune privilege of self-antigens during viral central nervous system infection. J. Immunol. *188*, 3678–3685.

Cervantes-Barragán, L., Lewis, K.L., Firner, S., Thiel, V., Hugues, S., Reith, W., Ludewig, B., and Reizis, B. (2012b). Plasmacytoid dendritic cells control T-cell response to chronic viral infection. Proc. Natl. Acad. Sci. USA *109*, 3012–3017.

Chyou, S., Ekland, E.H., Carpenter, A.C., Tzeng, T.C., Tian, S., Michaud, M., Madri, J.A., and Lu, T.T. (2008). Fibroblast-type reticular stromal cells regulate the lymph node vasculature. J. Immunol. *181*, 3887–3896.

Cupedo, T., Jansen, W., Kraal, G., and Mebius, R.E. (2004a). Induction of secondary and tertiary lymphoid structures in the skin. Immunity *21*, 655–667.

Cupedo, T., Lund, F.E., Ngo, V.N., Randall, T.D., Jansen, W., Greuter, M.J., de Waal-Malefyt, R., Kraal, G., Cyster, J.G., and Mebius, R.E. (2004b). Initiation of cellular organization in lymph nodes is regulated by non-B cell-derived signals and is not dependent on CXC chemokine ligand 13. J. Immunol. *173*, 4889–4896.

Cupedo, T., Vondenhoff, M.F., Heeregrave, E.J., De Weerd, A.E., Jansen, W., Jackson, D.G., Kraal, G., and Mebius, R.E. (2004c). Presumptive lymph node organizers are differentially represented in developing mesenteric and peripheral nodes. J. Immunol. *173*, 2968–2975.

De Togni, P., Goellner, J., Ruddle, N.H., Streeter, P.R., Fick, A., Mariathasan, S., Smith, S.C., Carlson, R., Shornick, L.P., Strauss-Schoenberger, J., et al. (1994). Abnormal development of peripheral lymphoid organs in mice deficient in lymphotoxin. Science *264*, 703–707.

Eberl, G., Marmon, S., Sunshine, M.J., Rennert, P.D., Choi, Y., and Littman, D.R. (2004). An essential function for the nuclear receptor RORgamma(t) in the generation of fetal lymphoid tissue inducer cells. Nat. Immunol. *5*, 64–73.

Finke, D., Acha-Orbea, H., Mattis, A., Lipp, M., and Kraehenbuhl, J. (2002). CD4+CD3- cells induce Peyer's patch development: role of alpha4beta1 integrin activation by CXCR5. Immunity *17*, 363–373.

Fletcher, A.L., Lukacs-Kornek, V., Reynoso, E.D., Pinner, S.E., Bellemare-Pelletier, A., Curry, M.S., Collier, A.R., Boyd, R.L., and Turley, S.J. (2010). Lymph node fibroblastic reticular cells directly present peripheral tissue antigen under steady-state and inflammatory conditions. J. Exp. Med. *207*, 689–697.

Fütterer, A., Mink, K., Luz, A., Kosco-Vilbois, M.H., and Pfeffer, K. (1998). The lymphotoxin beta receptor controls organogenesis and affinity maturation in peripheral lymphoid tissues. Immunity *9*, 59–70.

Gil-Cruz, C., Perez-Shibayama, C., Firner, S., Waisman, A., Bechmann, I., Thiel, V., Cervantes-Barragan, L., and Ludewig, B. (2012). T helper cell- and CD40-dependent germline IgM prevents chronic virus-induced demyelinating disease. Proc. Natl. Acad. Sci. USA *109*, 1233–1238.

Gunn, M.D., Kyuwa, S., Tam, C., Kakiuchi, T., Matsuzawa, A., Williams, L.T., and Nakano, H. (1999). Mice lacking expression of secondary lymphoid organ chemokine have defects in lymphocyte homing and dendritic cell localization. J. Exp. Med. *189*, 451–460.

Honda, K., Nakano, H., Yoshida, H., Nishikawa, S., Rennert, P., Ikuta, K., Tamechika, M., Yamaguchi, K., Fukumoto, T., Chiba, T., and Nishikawa, S.I. (2001). Molecular basis for hematopoietic/mesenchymal interaction during initiation of Peyer's patch organogenesis. J. Exp. Med. *193*, 621–630.

Junt, T., Scandella, E., and Ludewig, B. (2008). Form follows function: lymphoid tissue microarchitecture in antimicrobial immune defence. Nat. Rev. Immunol. *8*, 764–775.

Kägi, D., Ledermann, B., Bürki, K., Seiler, P., Odermatt, B., Olsen, K.J., Podack, E.R., Zinkernagel, R.M., and Hengartner, H. (1994). Cytotoxicity mediated by T cells and natural killer cells is greatly impaired in perforin-deficient mice. Nature *369*, 31–37.

Katakai, T., Hara, T., Lee, J.H., Gonda, H., Sugai, M., and Shimizu, A. (2004). A novel reticular stromal structure in lymph node cortex: an immuno-platform for interactions among dendritic cells, T cells and B cells. Int. Immunol. *16*, 1133–1142.

Kong, Y.Y., Yoshida, H., Sarosi, I., Tan, H.L., Timms, E., Capparelli, C., Morony, S., Oliveira-dos-Santos, A.J., Van, G., Itie, A., et al. (1999). OPGL is a key regulator of osteoclastogenesis, lymphocyte development and lymph-node organogenesis. Nature *397*, 315–323.

Koni, P.A., Sacca, R., Lawton, P., Browning, J.L., Ruddle, N.H., and Flavell, R.A. (1997). Distinct roles in lymphoid organogenesis for lymphotoxins alpha and beta revealed in lymphotoxin beta-deficient mice. Immunity *6*, 491–500.

Krautler, N.J., Kana, V., Kranich, J., Tian, Y., Perera, D., Lemm, D., Schwarz, P., Armulik, A., Browning, J.L., Tallquist, M., et al. (2012). Follicular dendritic cells emerge from ubiquitous perivascular precursors. Cell *150*, 194–206.

Kumar, V., Scandella, E., Danuser, R., Onder, L., Nitschké, M., Fukui, Y., Halin, C., Ludewig, B., and Stein, J.V. (2010). Global lymphoid tissue remodeling during a viral infection is orchestrated by a B cell-lymphotoxin-dependent pathway. Blood *115*, 4725–4733.

Link, A., Vogt, T.K., Favre, S., Britschgi, M.R., Acha-Orbea, H., Hinz, B., Cyster, J.G., and Luther, S.A. (2007). Fibroblastic reticular cells in lymph nodes regulate the homeostasis of naive T cells. Nat. Immunol. *8*, 1255–1265.

Lötzer, K., Döpping, S., Connert, S., Gräbner, R., Spanbroek, R., Lemser, B., Beer, M., Hildner, M., Hehlgans, T., van der Wall, M., et al. (2010). Mouse aorta smooth muscle cells differentiate into lymphoid tissue organizer-like cells on combined tumor necrosis factor receptor-1/lymphotoxin beta-receptor NF-kappaB signaling. Arterioscler. Thromb. Vasc. Biol. *30*, 395–402.

Lukacs-Kornek, V., Malhotra, D., Fletcher, A.L., Acton, S.E., Elpek, K.G., Tayalia, P., Collier, A.R., and Turley, S.J. (2011). Regulated release of nitric oxide by nonhematopoietic stroma controls expansion of the activated T cell pool in lymph nodes. Nat. Immunol. *12*, 1096–1104.

Malhotra, D., Fletcher, A.L., Astarita, J., Lukacs-Kornek, V., Tayalia, P., Gonzalez, S.F., Elpek, K.G., Chang, S.K., Knoblich, K., Hemler, M.E., et al.; Immunological Genome Project Consortium. (2012). Transcriptional profiling of stroma from inflamed and resting lymph nodes defines immunological hallmarks. Nat. Immunol. *13*, 499–510.

Mebius, R.E., Rennert, P., and Weissman, I.L. (1997). Developing lymph nodes collect CD4+CD3- LTbeta+ cells that can differentiate to APC, NK cells, and follicular cells but not T or B cells. Immunity *7*, 493–504.

Mueller, S.N., and Germain, R.N. (2009). Stromal cell contributions to the homeostasis and functionality of the immune system. Nat. Rev. Immunol. *9*, 618–629.

Ohl, L., Henning, G., Krautwald, S., Lipp, M., Hardtke, S., Bernhardt, G., Pabst, O., and Förster, R. (2003). Cooperating mechanisms of CXCR5 and CCR7 in development and organization of secondary lymphoid organs. J. Exp. Med. *197*, 1199–1204.

Onder, L., Scandella, E., Chai, Q., Firner, S., Mayer, C.T., Sparwasser, T., Thiel, V., Rülicke, T., and Ludewig, B. (2011). A novel bacterial artificial

chromosome-transgenic podoplanin-cre mouse targets lymphoid organ stromal cells in vivo. Front Immunol *2*, 50.

Onder, L., Danuser, R., Scandella, E., Firner, S., Chai, Q., Hehlgans, T., Stein, J.V., and Ludewig, B. (2013). Endothelial cell-specific lymphotoxin-β receptor signaling is critical for lymph node and high endothelial venule formation. J. Exp. Med. *210*, 465–473.

Randall, T.D., Carragher, D.M., and Rangel-Moreno, J. (2008). Development of secondary lymphoid organs. Annu. Rev Immunol. *26*, 627–650.

Siegert, S., Huang, H.Y., Yang, C.Y., Scarpellino, L., Carrie, L., Essex, S., Nelson, P.J., Heikenwalder, M., Acha-Orbea, H., Buckley, C.D., et al. (2011). Fibroblastic reticular cells from lymph nodes attenuate T cell expansion by producing nitric oxide. PLoS ONE *6*, e27618.

Sixt, M., Kanazawa, N., Selg, M., Samson, T., Roos, G., Reinhardt, D.P., Pabst, R., Lutz, M.B., and Sorokin, L. (2005). The conduit system transports soluble antigens from the afferent lymph to resident dendritic cells in the T cell area of the lymph node. Immunity *22*, 19–29.

Soriano, S.F., Hons, M., Schumann, K., Kumar, V., Dennier, T.J., Lyck, R., Sixt, M., and Stein, J.V. (2011). In vivo analysis of uropod function during physiological T cell trafficking. J. Immunol. *187*, 2356–2364.

Srinivas, S., Watanabe, T., Lin, C.S., William, C.M., Tanabe, Y., Jessell, T.M., and Costantini, F. (2001). Cre reporter strains produced by targeted insertion of EYFP and ECFP into the ROSA26 locus. BMC Dev. Biol. *1*, 4.

Turley, S.J., Fletcher, A.L., and Elpek, K.G. (2010). The stromal and haematopoietic antigen-presenting cells that reside in secondary lymphoid organs. Nat. Rev. Immunol. *10*, 813–825.

van de Pavert, S.A., and Mebius, R.E. (2010). New insights into the development of lymphoid tissues. Nat. Rev. Immunol. *10*, 664–674.

Vega, F., Coombes, K.R., Thomazy, V.A., Patel, K., Lang, W., and Jones, D. (2006). Tissue-specific function of lymph node fibroblastic reticulum cells. Pathobiology *73*, 71–81.

Veiga-Fernandes, H., Coles, M.C., Foster, K.E., Patel, A., Williams, A., Natarajan, D., Barlow, A., Pachnis, V., and Kioussis, D. (2007). Tyrosine kinase receptor RET is a key regulator of Peyer's patch organogenesis. Nature *446*, 547–551.

White, A., Carragher, D., Parnell, S., Msaki, A., Perkins, N., Lane, P., Jenkinson, E., Anderson, G., and Caamaño, J.H. (2007). Lymphotoxin a-dependent and -independent signals regulate stromal organizer cell homeostasis during lymph node organogenesis. Blood *110*, 1950–1959.

Wimmer, N., Huber, B., Barabas, N., Röhrl, J., Pfeffer, K., and Hehlgans, T. (2012). Lymphotoxin β receptor activation on macrophages induces cross-tolerance to TLR4 and TLR9 ligands. J. Immunol. *188*, 3426–3433.

Worbs, T., Mempel, T.R., Bölter, J., von Andrian, U.H., and Förster, R. (2007). CCR7 ligands stimulate the intranodal motility of T lymphocytes in vivo. J. Exp. Med. *204*, 489–495.

Yoshida, H., Honda, K., Shinkura, R., Adachi, S., Nishikawa, S., Maki, K., Ikuta, K., and Nishikawa, S.I. (1999). IL-7 receptor alpha+ CD3(-) cells in the embryonic intestine induces the organizing center of Peyer's patches. Int. Immunol. *11*, 643–655.